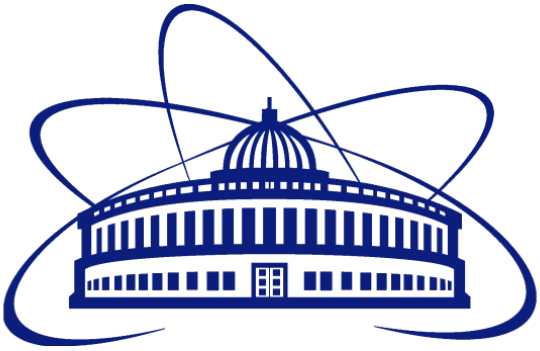

JOINT INSTITUTE FOR NUCLEAR REASEARCH

FLEROV LABORATORY OF NUCLEAR REACTIONS (FLNR)

FINAL REPORT ON THE INTEREST PROGRAMME

Prompt gamma-ray spectroscopy using segmented High-Purity Germanium (HPGe) detectors

Supervisor:

Dr. Aniruddha Dey

Student:

An Binh Le

University of Science

Vietnam National University, Ho Chi Minh City (VNU-HCM)

Participation period:

Feb 26 - Apr 14, Wave 10

Dubna, 2024

Contents

Abstract

This paper is the final report for the INTEREST program at wave 10 including a general perspective on prompt gamma-ray spectroscopy survey. The work is to evaluate the properties of gamma detection using four high purity Germanium (HPGe) crystals as single-crystal detectors and a combined (add-back) detector. The literature review on the interaction of gamma within the materials was accounted, giving a fundamental perception when come to comprehend the detection signal. The experiment set up includes six Clover detectors consisting of four HPGe crystals each, with two radiactive sources are ^{152}Eu and ^{133}Ba to generate the spectra. Subsequently, the spectral data was analysed by the support of Radware program to obtain the energy calibration curve, full width at half max (FWHM) and resolution at single-crystal and add-back mode. These parameters are the indicators in awaring the operational feature of detectors, which is depent on deposited energy. Due to modification between two modes, the detection efficiency was elucidated based on add-back factors (F), which showing a better gamma detection capability of Clover detectors when operates in add-back mode.

1 Introduction

Nuclei can undergo a variety of processes resulting in the emission of radiation of some form. The processes can be divided into two categories: radioactivity and nuclear reactions [14]. In a radioactive transformation, the nucleus spontaneously disintegrates to a different species of nuclei or to a lower energy state of the same nucleus with the emission of radiation of some sort. In a nuclear reaction, the nucleus interacts with another particle or nucleus with the subsequent emission of radiation as one of its final products. In many cases, some of the products are nuclei which further undergo radioactive disintegration. The radiation emitted in both of these processes may be electromagnetic or corpuscular. Among others, gamma-ray with high energy generally originate in the nucleus itself and chacracterize for specific nucleus as a fingerprint. For this reason, photon spectrometry is a widely used nuclear measurement technique for identifying and quantifying X- and gamma-emitting radionuclides in any kind.

One of the most potent instruments in experimental nuclear research is high resolution gamma-ray spectroscopy, which has been widely used to investigate a wide range of topics related to nuclear structure and reaction kinetics. The current study will offer a thorough understanding of the operation of gamma detectors and how to use them to extract different atomic characteristics of nuclie. The main goal is to comprehend the significance of a mount array of gamma detectors by studying the basic properties of a typical segmented High-Purity Germanium (HPGe) detector. The future of Gamma-ray spectroscopy measuring techniques worldwide is held by a large array of detectors made up of several types of segmented HPGe detectors.

2 Gamma-ray interaction mechanism

There are three major types play an important role in radiation measurements: photo-electric absorption, Compton scattering, and pair production. All these processes lead to the partial or complete transfer of the gamma-ray photon energy to electron energy. They result in sudden and abrupt changes in the gamma-ray photon history, in that the photon either disappears entirely or is scattered through a significant angle.

2.1 Photoelectric effect

The photoelectric effect (Figure 1) is the process in which an electromagnetic quantum of energy $h\upsilon$ ejects a bound electron from an atom or molecule and imparts to it an energy $h\upsilon - be$, be being the electron binding energy. Total absorption of the energy can only occur if the electron is initially bound in the atom, because a third body, the nucleus is necessary for conserving momentum. Let's assume a gamma having energy of E_γ and the momentum

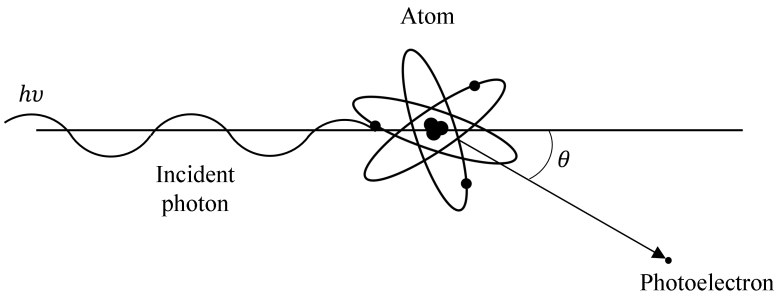

Figure 1. Photoelectric effect.

E_γ/c, coming to interact with a electron at rest. After absorbing all energy of the gamma, the final energy of the electron can be calculated using conservation law of momentum:

$$\begin{aligned} \overrightarrow{p'_e} &= \overrightarrow{p_e} + \overrightarrow{p_\gamma} \\ p'^{\,2}_e &= \left(\frac{E_\gamma}{c}\right)^2 \\ \left(p'_e c\right)^2 &= E_\gamma^2 \,, \end{aligned} \tag{1}$$

and conservation law of energy,

$$\begin{aligned} E'_e &= E_e + E_\gamma \\ E_0^2 + \left(p'_e c\right)^2 &= \left(E_0 + E_\gamma\right)^2 \\ 2E_0 E_\gamma &= 0 \,. \end{aligned} \tag{2}$$

Where p_e, p'_e are the momenta of electron before and after collision. The Equation 2 shows either the rest mass energy of the electron or the energy of incident gamma is equal to zero. This contradict with the initial assumption. Thus, a free electron cannot absorb a photon and become a photoelectron and the interaction probability will increase with the electron binding energy. Nevertheless, in order that the photoelectric interaction may take place, the individual photon energy must exceed the electron binding energy K_{ab} of the absorber [2].

The electron binding energies K_{ab} of the various elements are shown in Figure 2. This leads to sharp discontinuities in the photoelectric interaction probabilities at energies equal to the binding energies of the $K-$, $L-$, or $M-$shell electrons. When it is energetically possible, about 80% of the photoelectric interactions take place in the $K-$shell, and a large part of the remaining 20% takes place in the $L-$shell [11]. This photoelectric cross-section varies in a complex manner with E and with the value of Z of the absorber. The photoelectric process is the predominant mode of interaction for gamma-rays (or X-rays) of relatively low energy. The process is also enhanced for absorber materials of high atomic number Z. In case of

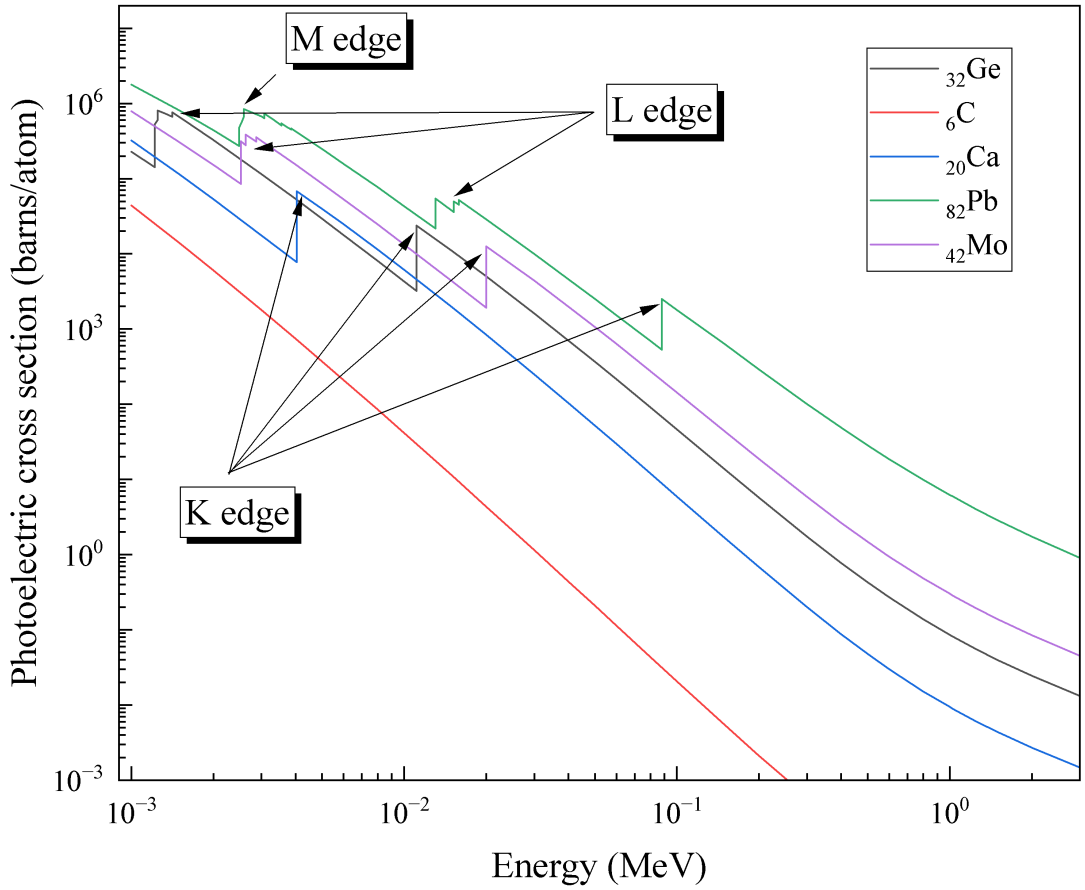

Figure 2. Photoelectric effect cross section of some elements depending on energy.

Lead (Pb), it shows a high photoelectric cross section was higher than other elements, but it is not a good choice for detector. The K edge of Germanium (Ge) has lower energy than that of Pb and has a smaller density. Further more, Pb generate more X-ray when coming to low energy region, corresponding to L- and M-edge, it makes the gamma spectrum more complicated. Ge is known as semiconductor, which act as insulators at low temperatures and conductors at higher temperatures. Thus, Ge is widely used as a detector material. No single analytic expression is valid for the probability of photoelectric absorption per atom over all ranges of E and Z, but a rough approximation is

$$\sigma_{\text{photo}} \cong \text{constant} \times \frac{Z^n}{E_\gamma^{3.5}}, \tag{3}$$

where the exponent n varies between 4 and 5 over the gamma-ray energy region of interest. This severe dependence of the photoelectric absorption probability on the atomic number of the absorber is a primary reason for the preponderance of high-Z materials in gamma-ray shields. Many detectors used for gamma-ray spectroscopy are chosen from high-Z

constituents for the same reason [8]. In addition to the photoelectron, the interaction also

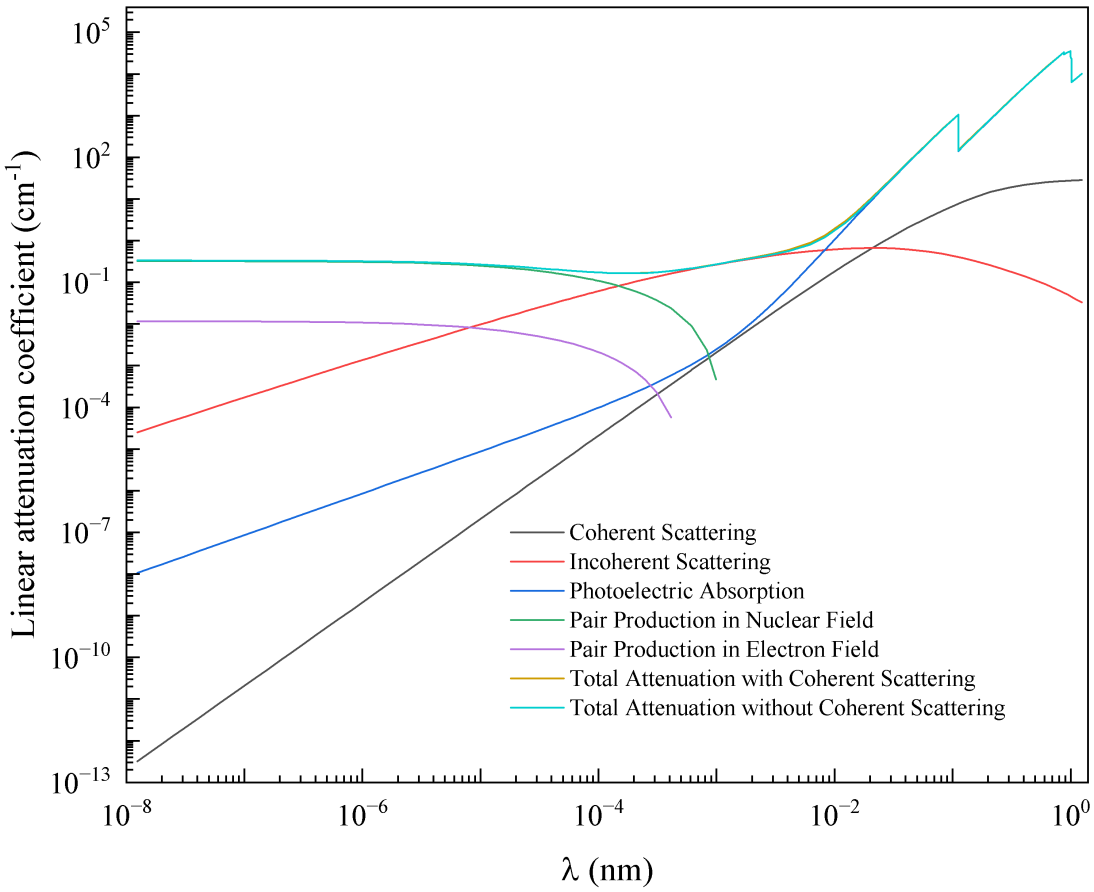

Figure 3. Linear absorption coefficient of Germanium as a function of photon wavelength.

creates an ionized absorber atom with a vacancy in one of its bound shells. This vacancy is quickly filled through capture of a free electron from the medium and rearrangement of electrons from other shells of the atom. Therefore, one or more characteristic X-ray photons may also be generated. Although in most cases these X-rays are reabsorbed close to the original site through photoelectric absorption involving less tightly bound shells, their migration and possible escape from radiation detectors can influence their response. In some fraction of the cases, the emission of an Auger electron may substitute for the characteristic X-ray in carrying away the atomic excitation energy.

2.2 Compton scattering

The Compton effect is a collision between a gamma-ray and an electron, which in this case may be either bound or free. In practical situations the scattering electrons are virtually all bound, although it is not a necessary condition for the Compton interaction. In the photoelectric effect just reviewed it is essential that the electron be bound so that the atom

may participate in the conservation of momentum. The photoelectric effect takes place almost entirely with the inner K or L electrons and is a relatively intense source of characteristic X-rays [15]. Compton scattering will generally involve the outer electrons, and does not produce a significant amount of K or L X-rays except in the light elements. There fore the energy of the photon being generally much higher than the binding energy of the electron in the atom, the electron can be considered as free.

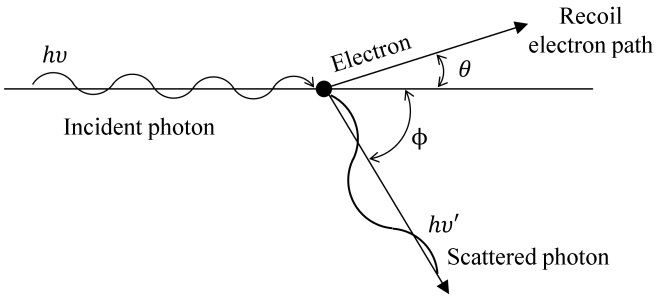

Figure 4. Compton scattering diagram.

Instead of giving up its entire energy, the photon transfers only part of its energy. The photon is degraded in energy and deflected from its original path. As Figure 4 shows, it makes an angle ϕ with its original direction, while the electron recoils in a direction making an angle θ with that of the incident photon. The trajectories of the incident photon, Compton scattered photon, and recoil electron occur always in one plane. The angle θ of emission of the electron is correlated with ϕ through

$$\cot\theta = (1+\alpha)\tan\frac{\phi}{2}\,, \tag{4}$$

where $\alpha = E/mc^2$. A useful and convenient relation derived from relativistic conditions for conservation of momentum for this interaction is expressed as follows:

$$\overrightarrow{p_i} = \overrightarrow{p_f} + \overrightarrow{p_e} \tag{5}$$

$$p_e^2 = p_i^2 + p_f^2 - 2p_i p_f \cos\phi\,, \tag{6}$$

with the substitution of $p = E/c$,

$$E_e^2 = E_i^2 + E_f^2 - 2E_i E_f \cos\phi\,. \tag{7}$$

And energy equations,

$$E_i + E_0 = E_f + \sqrt{E_0^2 + E_e^2} \tag{8}$$

$$E_e^2 = \left(E_i - E_f + E_0\right)^2 - E_0^2\,, \tag{9}$$

from the Equation 7, it can be obtained that:

$$\left(E_i - E_f + E_0\right)^2 - E_0^2 = E_i^2 + E_f^2 - 2E_iE_f\cos\phi \tag{10}$$

$$E_0\left(E_i - E_f\right) = E_iE_f\left(1 - \cos\phi\right) \tag{11}$$

$$h\upsilon' = \frac{h\upsilon}{1 + \frac{h\upsilon}{mc^2}\left(1 - \cos\phi\right)} \tag{12}$$

where m represents the rest mass and $E_0 = mc^2$ (0.511 MeV) the rest mass energy of the electron. E_i and E_f are the initial, final energy of photon, respectively. The momentum of electron, photon before and after collision are p_e, p_i and p_f, correspondingly. The energy T of the scattered electron equals the difference between the original photon energy E and the scattered photon energy E'.

$$T = \frac{\alpha E(1 - \cos\phi)}{1 + \alpha(1 - \cos\phi)} \tag{13}$$

From Equation 4 and 12, it appears that the energies of the scattered electrons range from zero $\phi = 0°, \theta = 90°$ up to a maximum value $\phi = 180°, \theta = 0°$ (Figure 5). This maximum value is the so-called Compton edge:

$$T_m = \frac{1}{1 + \frac{1}{2\alpha}} \tag{14}$$

The cross section for Compton scattering was one of the first to be calculated using quantum electrodynamics and is known as the Klein-Nishina formula:

$$\frac{\mathrm{d}\sigma}{\mathrm{d}\omega} = \frac{r_0^2}{2}\frac{1 + \cos^2\phi}{|1 + \alpha(1 - \cos\phi)|^2}\left[1 + \frac{\alpha^2(1 - \cos\phi)^2}{(1 + \cos^2\phi)\,|1 + \alpha(1 - \cos\phi)|}\right]. \tag{15}$$

The total Compton cross-section obtained by integrating 15 over all scattering angles is

$$\sigma_T = 2\pi r_0^2\left[\frac{1 + \alpha}{\alpha^2}\left|\frac{2(1 + \alpha)}{1 + 2\alpha} - \frac{\ln(1 + 2\alpha)}{\alpha}\right| + \frac{\ln(1 + 2\alpha)}{2\alpha} - \frac{1 + 3\alpha}{(1 + 2\alpha)^2}\right] \ \text{cm}^2/\text{electron}, \tag{16}$$

where r_0 is the classical electron radius, $r_0 = e^2/mc^2 = 2.818 \times 10^{-13}$ cm.

Equations 15 and 16 have all been derived on the assumption that the scattering electrons are free and initially at rest. This is not true in the practical situation. Electrons of matter are bound, and they possess energy and momentum. Resulting in the Klein-Nishina formula's yielding computed cross-sections which are too high. But in most prac tical cases when the Compton interaction is predominant, the energy of the incident photon is much greater than the electron binding energies.

From Figure 4 it is seen that a single Compton interaction absorbs only a portion of the

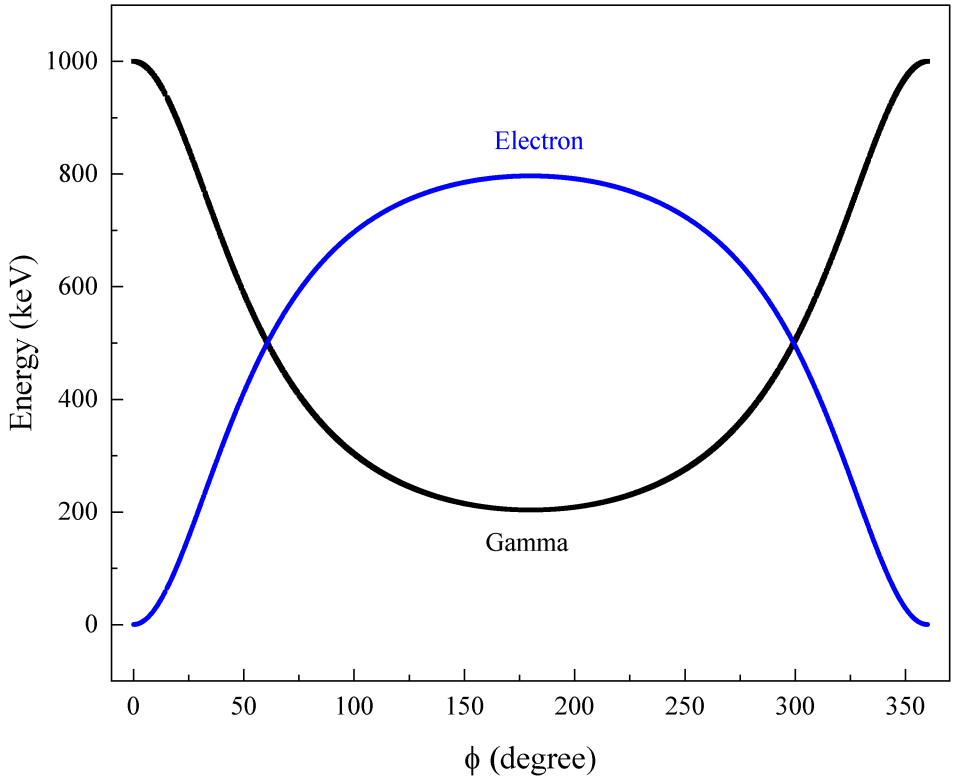

Figure 5. Energy of scattered photon and recoil electron as a function of cosine (1 MeV incident photon).

incident photon energy. The fraction of energy observed in any particular interaction is a function of the incident photon energy and the scattering angle. The angular distribution becomes more peaked in the forward direction the more the photon energy is increased (Figure 6).

At low incident photon energy, where the probable energy transfer per Compton interaction is low, the Compton cross-section becomes subordinate to the photo electric process. The Compton scattering cross-section is approximately proportional to E^{-1} at energies exceeding 0.5 MeV Thus it falls off less rapidly than the photoelectric absorption. Because the atomic Compton cross-section can be expressed as the sum of the cross-sections of the electrons $\sigma_a = Z_e\sigma$, the Compton attenuation coefficient is given by

$$\sigma_{\text{compton}} = N(Z/A)_e\sigma_a\rho. \tag{17}$$

Where N is Avogadro's number, Z is the number of electron, A is the atomic number and ρ is density of material. Thus σ is nearly independent of the nature of the absorber because $Z/A = 0.45 \pm 0.05$ [12] for almost all elements. In Figure 3 the Compton mass attenuation coefficient as plotted for Germanium for instance [6], can be applied to other absorbers.

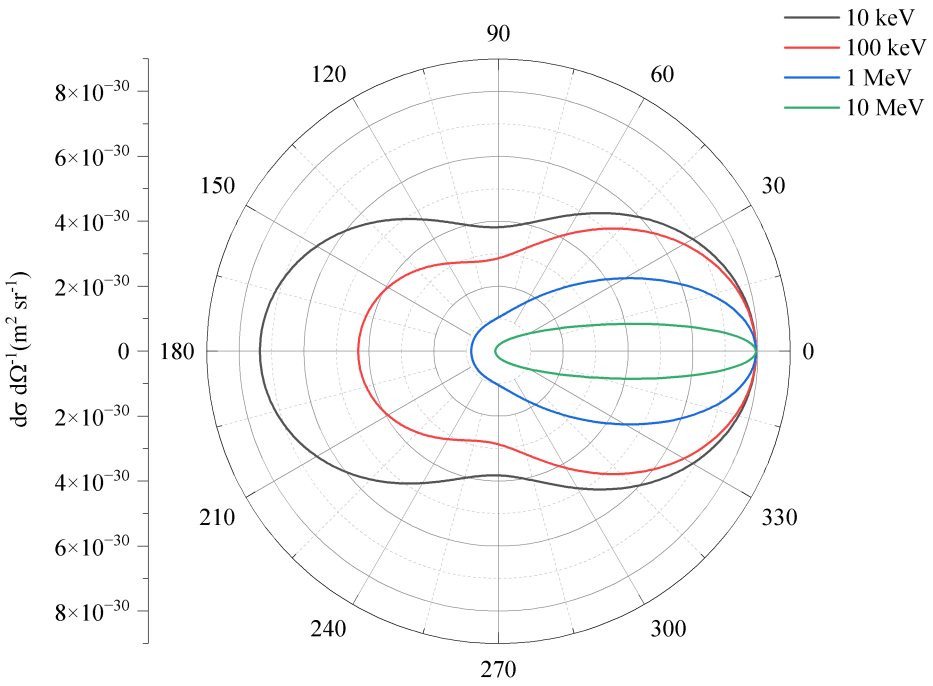

Figure 6. Compton effect. Differential cross-section per unit solid angle for the number of photon scattered at the angle ϕ.

2.3 Pair production

Above the incident photon energy of $2mc^2$ (1.022 MeV), pair production, the third major interaction mode of gamma quanta with matter becomes increasingly more important for increasing photon energies. The energy $2mc^2$ is a threshold for the process, and provides the rest mass energy necessary to create the positron-negatron pair. Figure 7 shows schematically the pair production. The interaction of an incident photon with a negatron converts it from a negative to a positive energy state and creates a hole (positron) and an electron.

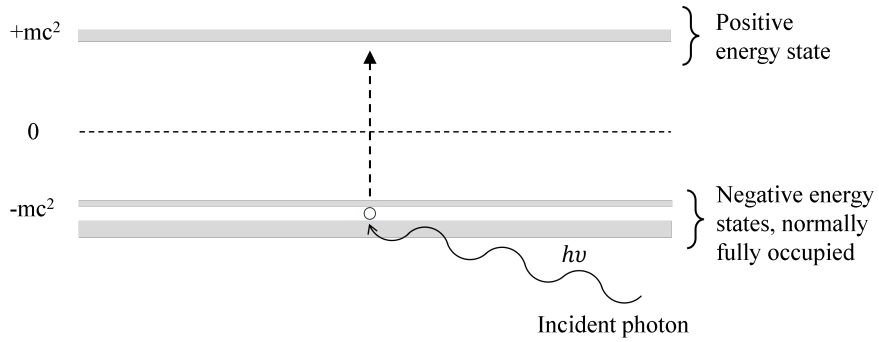

Figure 7. Pair production.

The difference between the incident photon energy and 1.022 MeV is divided between the created pair. The pair production attenuation coefficient σ_{pair} is proportional to Z^2/A. Above the threshold energy the probability for pair production increases slowly with increasing energy but above 4 MeV it becomes approximately proportional to $\log E$. At high energies pair production becomes the most important process (Figure 3).

The pair production may take place also in the Coulomb field of an orbital electron, resulting in the production of a triplet, that is the positron and the electron of the created pair, plus the electron in whose Coulomb field the process took place and which is ejected from the atom. The triplet production is of minor importance compared with pair produc tion in the nuclear Coulomb field, because the threshold energy for triplet production is $4mc^2$. The cross-section for this process for a material of atomic number Z proves to be Z^{-1} times the cross-section for pair production in the nuclear field.

The pair production process may be visualized according to the Dirac theory as follows: The relativistic wave equation for a free electron indicates that both positive and nega tive energy states $\geq \left|mc^2\right|$ exist. Since we do not observe free transitions of electrons from positive to negative energy states, it is assumed that all the negative energy states are occu pied by a sea of electrons. The exclusion principle then accounts for the failure of free electrons to annihilate, as no transition can be made to the fully occupied negative energy states.

When a negatron in the positive energy states fills the hole in the negative energy states, we have the annihilation of a pair of electrons. Annihilation of the positron-negatron pair generally does not occur until practically all the positron kinetic energy has been dissipated by ionization or radiative (bremsstrahlung) processes. Then two annihilation photons, each with 0.511 MeV energy, are emitted at approximately 180° with respect to each other, but nevertheless random with respect to the original photon direction. This annihilation radiation produces two additional escape peaks in the detectors response curves at 0.511 MeV intervals.

2.4 Other interactions

To describe the interaction of electromagnetic radiation with matter one can briefly say that the photons can interact with the following carriers of electricity:

a) With bound atomic electrons.

b) With free electrons (individual electrons).

c) With Coulomb fields (of nuclei or electrons).

d) With nucleons (individual nucleons or a whole nucleus).

These types of interaction may lead to one of three effects which are as follows:

(i) Complete absorption of a photon.

(ii) Elastic scattering.

(iii) Inelastic scattering.

Theoretically, therefore there are twelve processes for the absorption and scattering of gamma-rays possible [3]. However, in the energy range about 10 keV to about 10 MeV, most of the interactions result in one of the following processes.

1) At low energies the photoelectric effect (ia) predominates. A photon gives up all its energy to a bound electron. The electron uses part of the energy to overcome its binding to the atom and it takes the rest as kinetic energy.

2) The photon may be scattered by atomic or individual electrons, in another direction with or without loss of energy. At photon energies which exceed widely the binding energies of the electrons the photons are scattered as if the electrons were free and at rest. This is called the Compton effect (ic + iic), and it is the dominant mode of interaction around 1 MeV.

3) If the energy of the incident photon exceeds 1.022 MeV pair production (iiia) becomes possible. In the coulomb field of a charged particle an electron pair is created with total kinetic energy equal to the photon energy minus the rest mass energy of the two particles ($2mc^2$ = 1.022 MeV).

Although for gamma spectrometric measurements only photoelectric effect, Compton effect, and pair production are significant, also the elastic or coherent scattering (ib) may be important at low photon energies (up to 100 keV). Especially the more tightly bound electrons of the heavy elements favour this coherent scattering. Hence this coherent scattering interaction has long been the basis of X-ray crystallography. Each electron in the crystalline material is a source of coherently scattered radiation. A special effort must be made to reduce the undesirable characteristic X-ray background originating from the photoelectric interactions.

3 Data processing and analysis

3.1 Energy calibration

Energy calibration was performed before acquisition of the spectrum as part of the setting up procedure. This step is to convert the ouput ADCs signal, which is channel number, to energy value while keeping the counts. As shown in Figure 8, the initial spectra have some fluctuation in channel number that make difficult to peform further works. For example, the

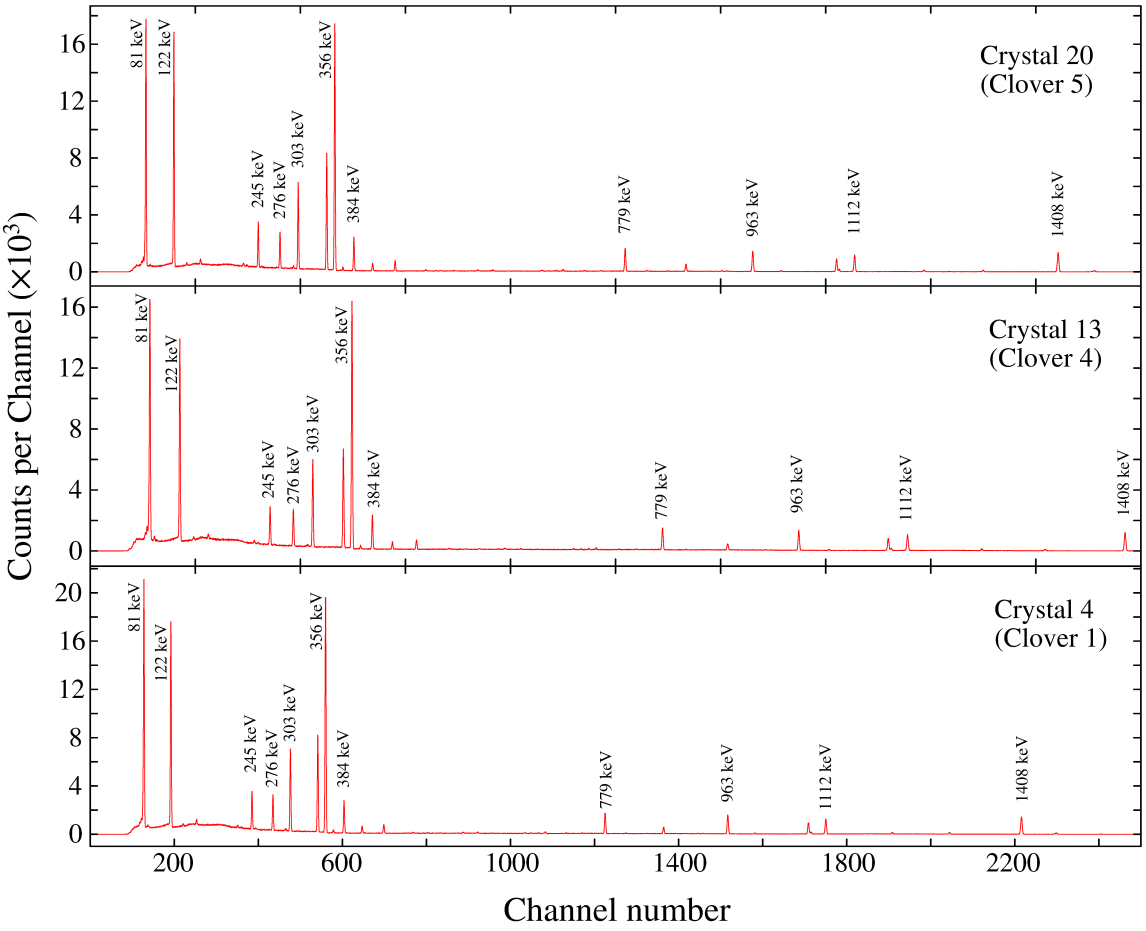

Figure 8. Spectra of peaks from ^{152}Eu and ^{133}Ba calibration sources.

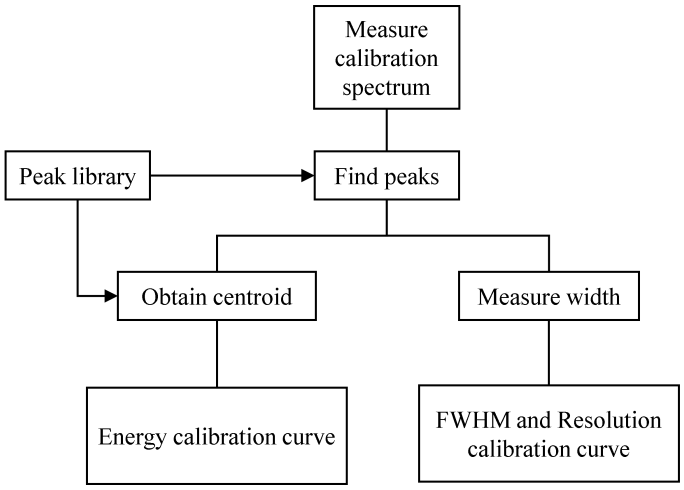

Figure 9. Flow chart for energy, FWHM and resolution peak calibration.

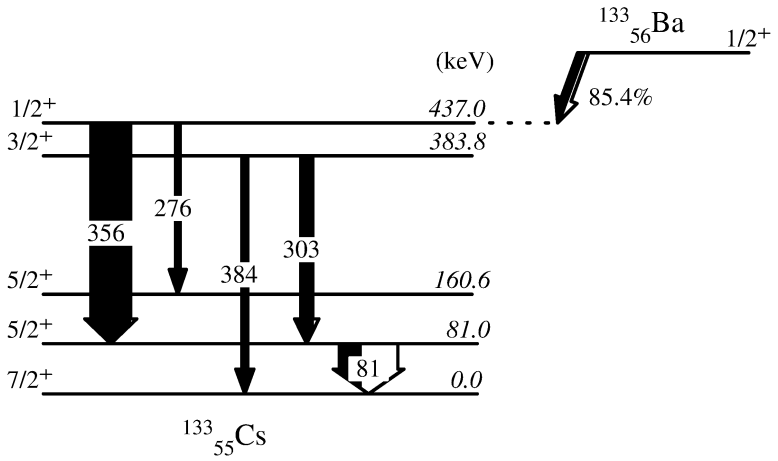

Figure 10. Five of the gamma energy from the decay of ^{133}Ba isotope were used to calibrate.

spectra of multiple crystals will be added to make a sum spectrum to find the mean add-back factor (F). Therefore, the spectra must be synchronized in term of channel. In some cases, the MCA calibration may only be rudimentary and a more precise calibration might be required before analysis of the spectra. Energy calibration by Radware involves the following steps (Figure 9):

- Measure the spectrum of a radioactive source which emits gamma-rays at precisely known energies.
- Open spectrum with Radware program and zoom on the desired peaks.
- Call the fitting fuction by 'af' or 'nf' command.
- Get the fitted peak centroids on the system terminal.
- Supply the precise energies of the selected peaks.

For this purpose the channel position of the maximum of each photo peak must be plotted versus the gamma-ray energy. A best fit through these data gives the energy corresponding to each channel in the multichannel analyzer. With good detectors a straight line is obtained; However, due to inherent nonlinearities in the detector or recording system this calibration may not be perfectly linear or pass exactly though the origin of the diagram. The construction of decay level scheme was carried out by gls feature in Radware. There are 16 gamma energy peaks from radioactive sources ^{152}Eu and ^{133}Ba were used to calibrate the crystals. Level scheme of ^{133}Ba isotope is shown in Figure 10, and that of ^{152}Eu for two decay channel (Figure 11, **??**), the thickness of transition arrows is proportional to their intensities.

The energy calibration consists in the experimental determination of a function, usually a first degree polynomial, describing the energy dependence of the channel number in the spectrum:

$$f(x) = A + Bx \tag{18}$$

$$f(x) = A + Bx + Cx^2 \tag{19}$$

Where $f(x)$ is the gamma-ray energy, x is the spectral channel number for the center of the peak corresponding to $f(x)$ (usually the channel with the maximum number of counts), while A, B and C are the constants to be determined for calibration. In some instances, a higher-order polynomial fit may be allowed and could provide a more precise fit, as shown in Figure 14. However, care should be taken. It has no theoretical reason to suppose that the energy relationship of any amplifier or ADC combination is quadratic. In fact, they are designed to be linear. The specification sheets for amplifiers and ADCs have noticed a serious non-linearity only at the extremities of the linear range [10]. For this reason, the linear correlation of the energy and channel number was found to display the difference in deviation (Figure 13). Without a theoretical basis, curve fitting is merely a mathematical estimation to achieve a more precise fit to the experimental data. There is a common between two fitting fuction that the deviation has increased in lower energy region, and decreased when come to the higher lateral part. The deviation of linear function cause a slight difference from quadratic one, although coefficcient of determination in both instances approximatle approaching to 1. Moreover, the quadratic funtion in Figure 14 could be reduce to linear by neglecting the slop factor of x^2 due to the extremly small value. Figure 15 displayed the spectra of crystal 1, 2 and 3 with the peaks correspondingly aligned at the same position, after applying energy calibration.

3.2 Calculation of full width at half max (FWHM)

For detectors which are designed to measure the energy of the incident radiation, the most important factor is the energy resolution. This is the extent to which the detector can distinguish two close lying energies. The resolution is usually given in terms of the full width at half maximum of the peak (FWHM). Energies which are closer than this interval are usually considered unresolvable. The resolving power of semiconductor gamma-ray detectors is mostly specified for the 1.33 MeV radiation of ^{60}Co. The energy resolution capabilities of semiconductor detectors are not always reached in practice. The resolving power which is obtained depends partly on the amplifying equipment, on noise sources in the detector, and on the charge collection. Unfortunately, the results explicitly displayed by Radware program on the terminal are widths. The FWHM values and its error must be calculated through width

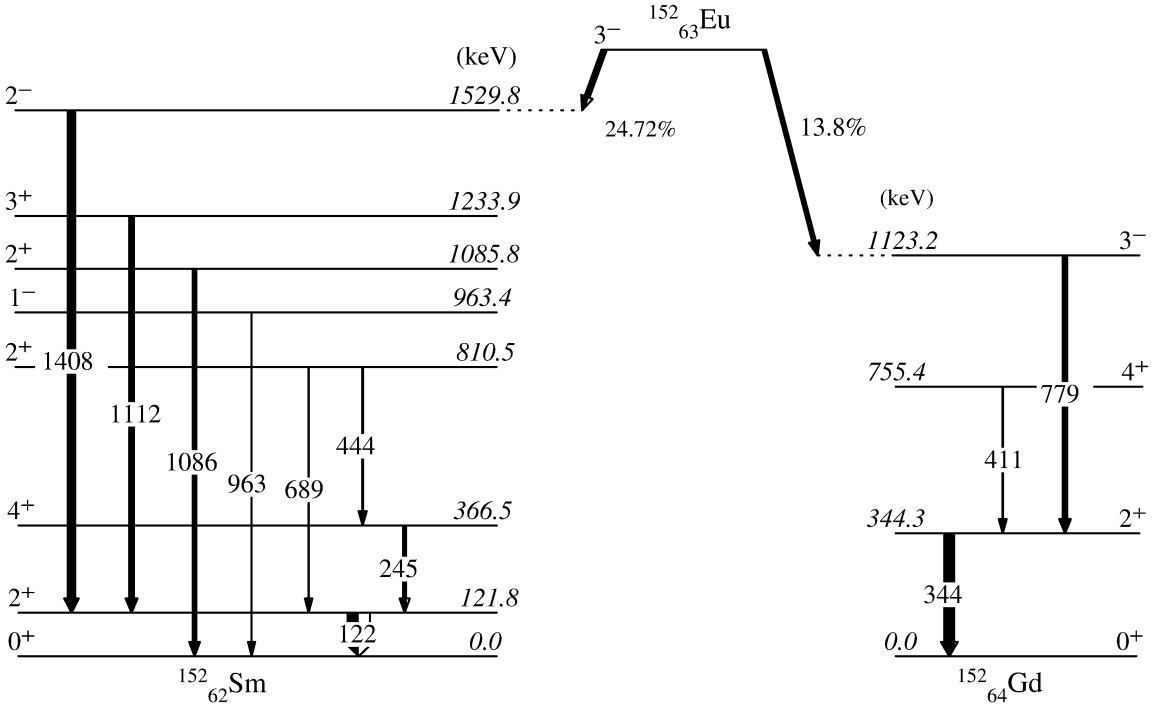

Figure 11. ^{152}Eu disintegrates 72.1% (left band) by electron-capture and 27.19% by minus beta emission (right band).

before calibration:

$$\text{FWHM} = \text{Width}\sqrt{\frac{\ln 2}{2}} \tag{20}$$

$$\Delta_{\text{FWHM}} = \Delta_{\text{Width}}\sqrt{\frac{\ln 2}{2}}. \tag{21}$$

Radware program use Gaussian distribution as its fitting method. The shape of the Gaussian is depend on the significance of σ as a measure of the distribution width. As shown before that the standard deviation corresponds to the half width of the peak at about 60% of the full height. However, the full width at half maximum (FWHM) is often used instead. This is somewhat larger than σ and can easily be shown to be FWHM = $2\sigma\sqrt{2\ln 2}$ and Width = 4σ, which finally make up to Equation 20.

Corresponding to energy calibration, the FWHM must be also plotted against the gamma-ray energy. There are various mathematical models for fitting these parameters. In fact, there is no theoretical justification for any of these alternative equations. The quadratic has a particular failing in that the statistical scatter of points can lead to an FWHM curve that curls upwards rather than downwards. In this project, the relation between enrgy and FWHM was fitted by the power function due to its coefficient of relation r^2 and reduced chi-squared χ^2/ndf gives better values. The formation of data points (Figure 12) seems to be linear.

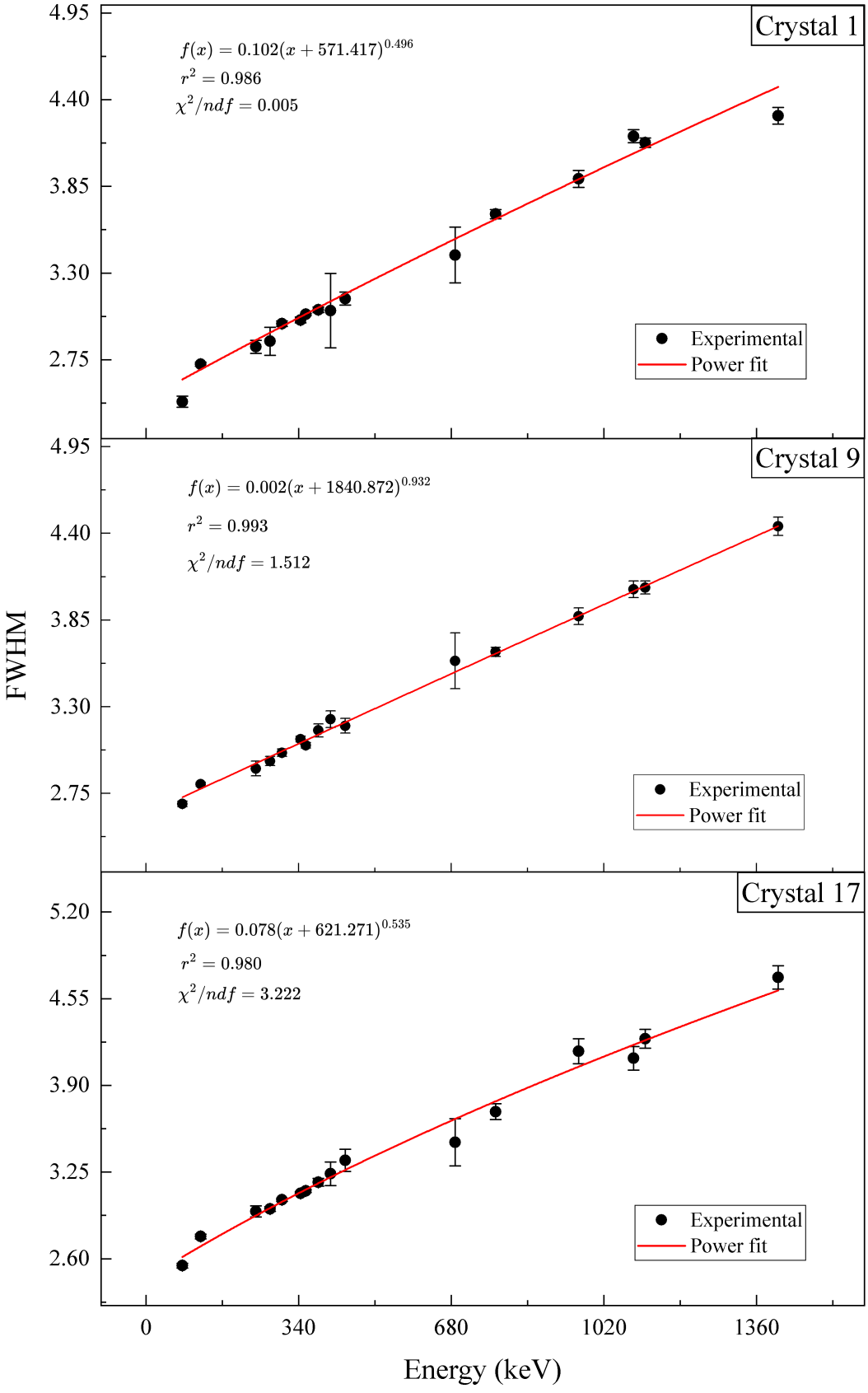

Figure 12. Power calibration curve of crystal 1 (Clover 1), 9 (Clover 3) and 17 (Clover 5), showing the depenence of FWHM to energy of gamma.

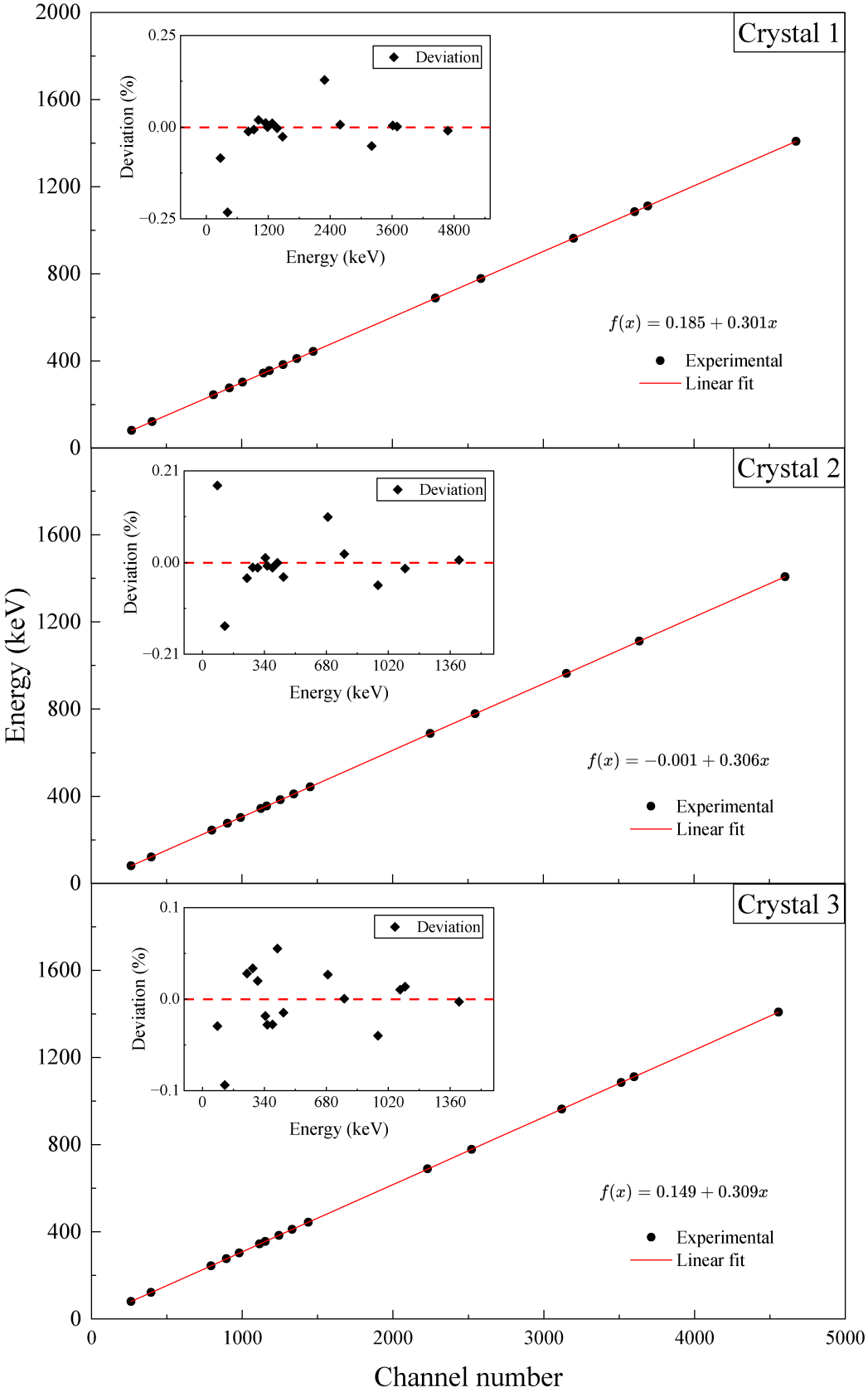

Figure 13. Linear calibration curve and deviation of crystal 1, 2 and 3 (Clover1).

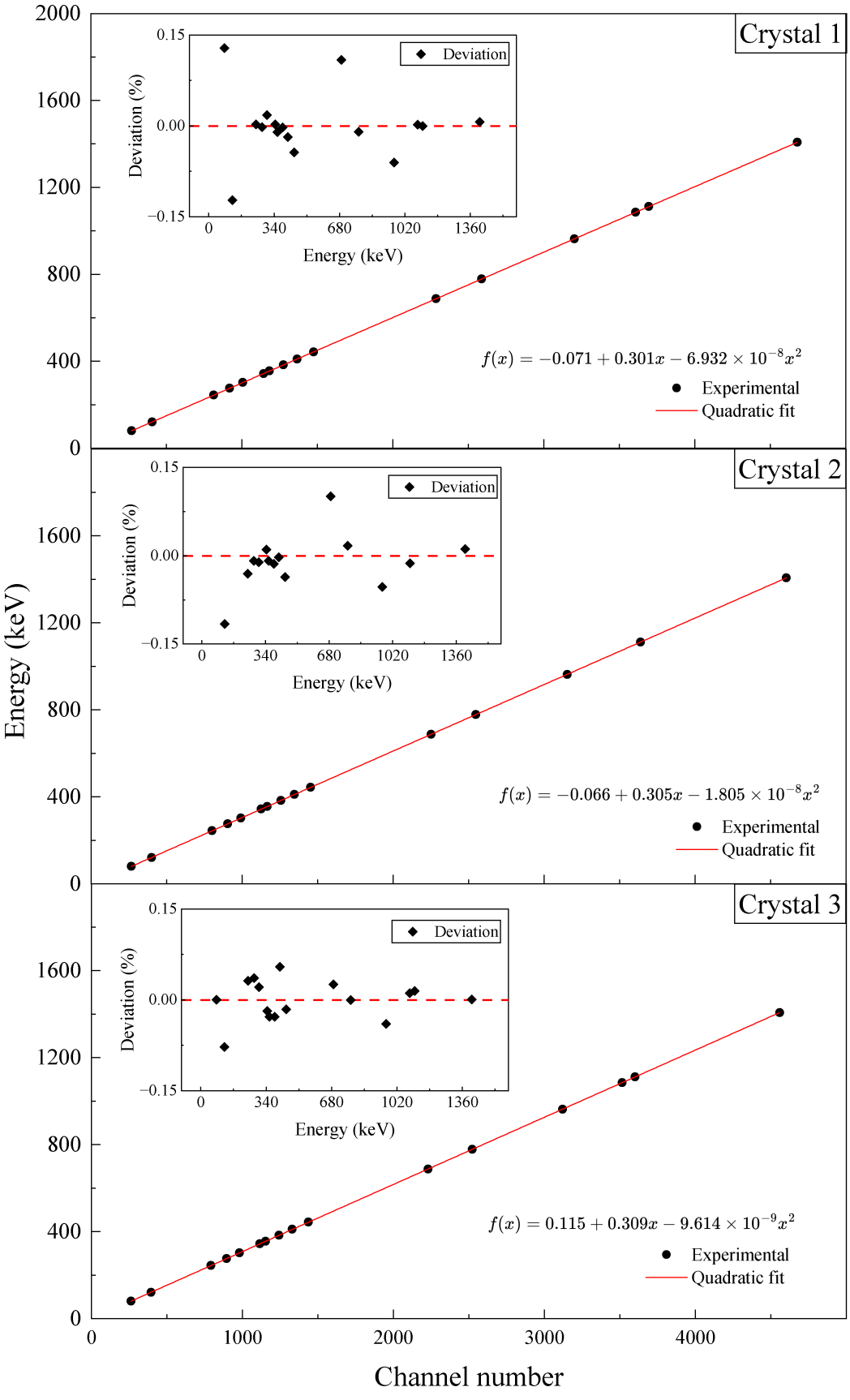

Figure 14. Quadratic calibration curve and deviation of crystal 1, 2 and 3 (Clover1).

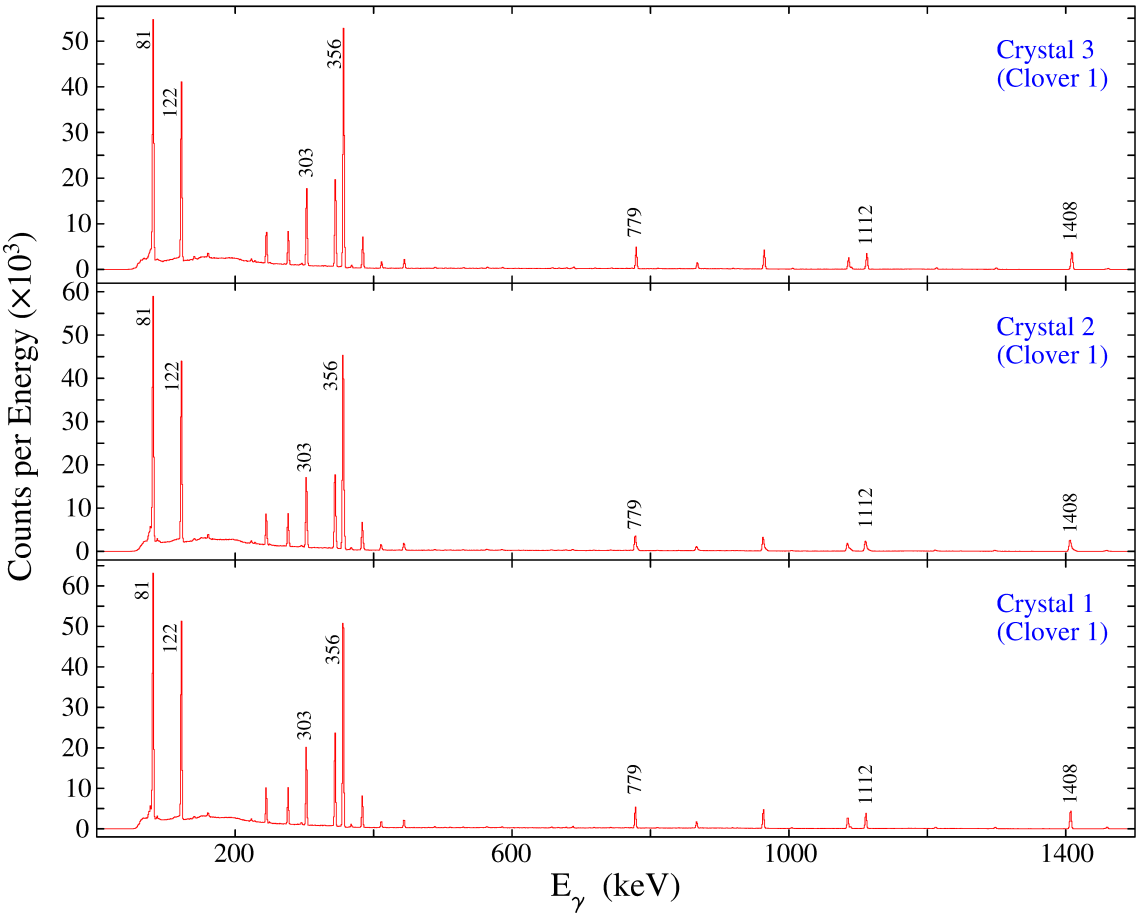

Figure 15. Yield spectra after calibration.

However, linear fitting cause worse statistical results. Some previous researches suggestted using power funtion for fitting this relation [9, 4, 5].

3.3 Add-back mode

Ultimately, all the spectra of the same Clover will be added to make a sum spectrum. The add-back spectrum of an individual cluster also obtained when opearating at correspoding mode. Two type of spectra are shown in the Figure 16 for clarification. The sum spectrum was formed by ordinarily adding all the counts of four crystals without considering the interaction of gamma. This would increase the count of photoelectric with others effect including noise. But in the add-back spectrum, the photopeaks were enhanced in counts due to the filter summation. Any deposition of gamma-ray within a given time and recorded in four crystal will be added to photoelectric signal. As shown in Figure 16, the Compton background in each of the above spectra will be more than the Compton background in each detector if there was only one crystal in the experiment. This increase in the Compton background is due to Compton scattering from any one crystal to the second, third or even fourth crystal. In this

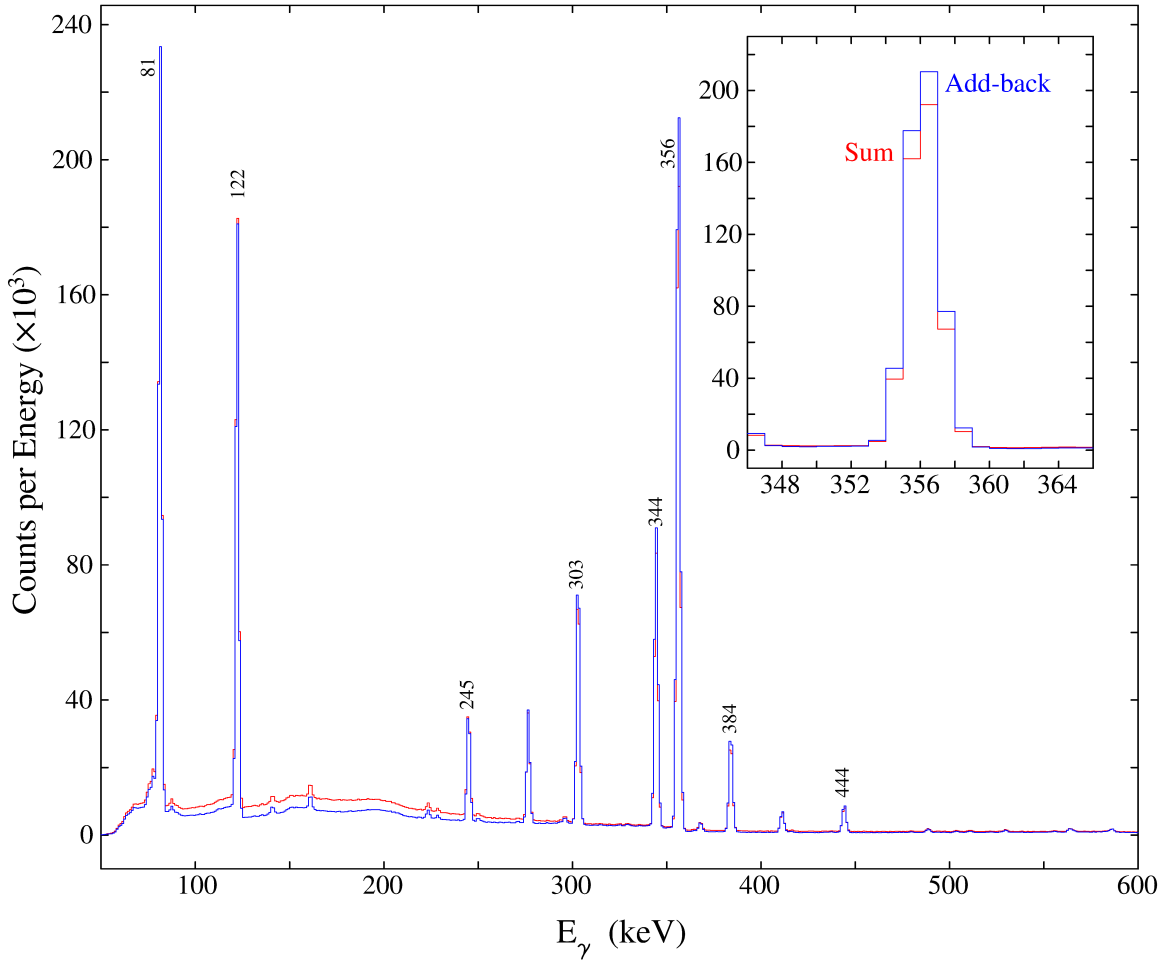

Figure 16. Comparison between sum (red line) and add-back spectrum (blue line).

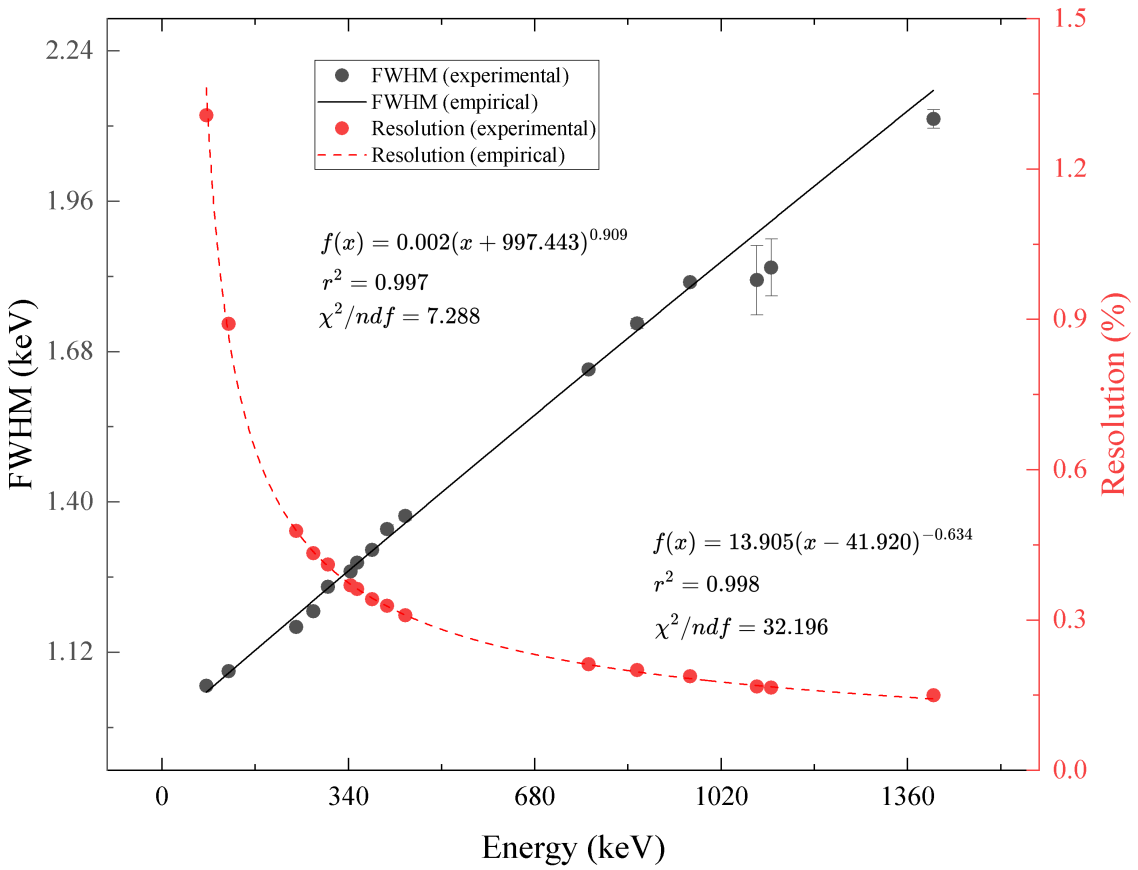

Figure 17. FWHM and Resolution of Clover 1 detector in add-back mode.

situation, some fraction of y-rays lose their full energy as Compton events in two or more detectors. These events can be recovered into the photopeak by adding the outputs of all the four detectors. The photopeak intensity in this add mode will, therefore, increase by more than a factor of four. It is also seen that the maximum addition of Compton events takes place from the low-energy region. Therefore, the reduction in the Compton background is more evident in the low-energy region < 500 keV [7].

3.4 Add-back factor

In order to have the evaluation on the mean add-back factor F, these spectra will be fitted by choosing a number of specific gamma peaks to get the areas as in the previous section. The mean add-back factor F is defined as the ratio of area of a peak in add-back spectrum

and that of a respective peak in the sum spectrum,

$$F = \frac{A_{\text{add-back}}}{A_{\text{sum}}}, \tag{22}$$

$$\Delta_{\text{F}} = F\sqrt{\left(\frac{\Delta A_{\text{add-back}}}{A_{\text{add-back}}}\right)^2 + \left(\frac{\Delta A_{\text{sum}}}{A_{\text{sum}}}\right)^2} \tag{23}$$

where $A_{\text{add-back}}$ is the area of the add-back peaks and A_{sum} is the area of peaks in the sum spectrum. The gamma-ray spectra were generated add-back events by adding the energies detected in each of the detectors. Several Compton events belonging to the group, where the total gamma-energy is lost in two or more detectors, will move to the photopeak as a result of the above addition. This gives rise to a higher photopeak efficiency where all spectra obtained above are added together. The full width at half max (FWHM) of Clover 1 detector is plotted in Figure 17 incorporate with resolution. The reduced chi-squared χ^2/ndf of fitting FWHM in add-back mode is higher than that of each crystal (Figure 12) with the same fitting fuction. Thus, it is expected a worsening of FWHM in the add-back mode.

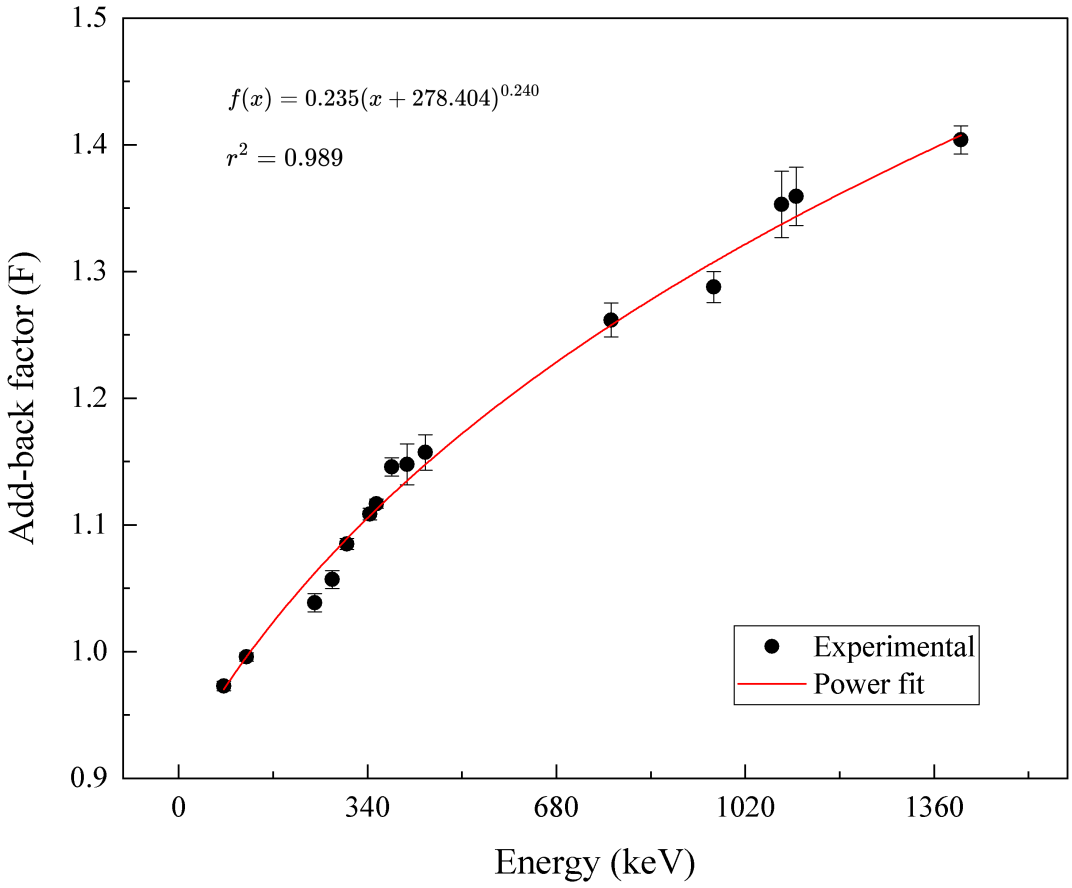

Figure 18. Mean add-back factor as a function of energy.

4 Summary

The assessment of featured operation of Clover detectors at single-crystal and add-back mode is done. This includes the energy calibration by using the Radware program to measure the spectrum (gf3) and generation (gls) of level scheme for ^{152}Eu, ^{133}Ba. These standard radioactive sources were used throughout the project to find the characteristic FWHM and resolution for each crystal and the detector at add-back mode. Moreover, the relation between parameters is fitted in the same mathematical function for a clear comparison. Finally, the mean add-back factor is deduced from the areas of photoelectric. This test results show that clover detector, when used in the add-back mode gives better peak/Compton ratio, thus increasing the photopeak efficiency, especially at higher enrgies. The Compton background in the low-energy region is reduced and FWHMs are poorer compared to a single HPGe detector. Thanks to its approaching to true detected signal, Clover detectors could be designed for more than four crystal to enhance the detection efficiency and used for many applications [1], especially in the energy region > 2 MeV [13].

5 Acknowledgement

I would like to express my gratitude to the INTEREST team for creating such an opportunity for me to join the most intriguing scientific project, which brings me insight and advantageous skills for my development as a young researcher. Additionally, the success of this project could not have been possible without the supportive and devoted guidance of Dr. Aniruddha Dey.

References

[1] F. Beck. Etude des transitions electromagnetiques dans les noyaux 207tl 13c 12b et mn par des methodes de correlations angulaires distributions angulaires et polarisation plane de rayons gamma. In *ANNALES DE PHYSIQUE*, volume 1, page 503. EDP SCIENCES 7, AVE DU HOGGAR, PARC D ACTIVITES COURTABOEUF, BP 112, F-91944 . . . , 1966.

[2] K. Buchtela. Radiochemical methods — gamma-ray spectrometry. In P. Worsfold, A. Townshend, and C. Poole, editors, *Encyclopedia of Analytical Science (Second Edition)*, pages 72–79. Elsevier, Oxford, second edition edition, 2005.

[3] C. Davisson. Interaction of γ-radiation with matter. In *Alpha-, beta-and gamma-ray spectroscopy*, pages 37–78. Elsevier, 1968.

[4] N. Demir and Z. N. Kuluöztürk. Determination of energy resolution for a nai (tl) detector modeled with fluka code. *Nuclear Engineering and Technology*, 53(11):3759–3763, 2021.

[5] J. K. Hartwell, R. J. Gehrke, and M. E. McIlwain. Performance comparison of four compact room-temperature detectors-two cadmium zinc telluride (czt) semiconductor detectors, a lacl/sub 3/(ce) scintillator, and an nai (tl) scintillator. In *IEEE Symposium Conference Record Nuclear Science 2004.*, volume 2, pages 856–860. IEEE, 2004.

[6] N. institute of Standards and T. (NIST). Xcom: Photon cross sections database. *https://physics.nist.gov/PhysRefData/Xcom/html/xcom1.html*, 2010. (Date Accessed: 22 March 2024).

[7] P. Joshi, H. Jain, A. Medhi, S. Chattopadhyay, S. Bhattacharya, and A. Goswami. Study of the characteristics of a clover detector. *Nuclear Instruments and Methods in Physics Research Section A: Accelerators, Spectrometers, Detectors and Associated Equipment*, 399(1):51–56, 1997.

[8] G. F. Knoll. *Radiation detection and measurement; 4th ed.* Wiley, New York, NY, 2010.

[9] C. Lee and H. R. Kim. Gamma-ray sensor using $YALO_3$ (ce) single crystal and cnt/peek with high sensitivity and stability under harsh underwater conditions. *Sensors*, 21(5):1606, 2021.

[10] M. A. Mohammedali, Q. Al-Gayem, et al. An accurate and fast method for improving adc nonlinearity. *Applied Computational Intelligence and Soft Computing*, 2023, 2023.

[11] F. Muleri et al. Expectations and perspectives of x-ray photoelectric polarimetry. 2009.

[12] C.-K. Qiao, J.-W. Wei, and L. Chen. An overview of the compton scattering calculation. *Crystals*, 11(5):525, 2021.

[13] M. S. Sarkar, P. Datta, I. Ray, C. Dey, S. Chattopadhyay, A. Goswami, P. Banerjee, R. Singh, P. Joshi, S. Paul, et al. Characteristics of a compton suppressed clover detector up to 5mev. *Nuclear Instruments and Methods in Physics Research Section A: Accelerators, Spectrometers, Detectors and Associated Equipment*, 491(1-2):113–121, 2002.

[14] G. R. Satchler. *Introduction to Nuclear Reactions*, pages 21–88. Palgrave Macmillan UK, London, 1990.

[15] L. J. Verhey and P. L. Petti. 7 - principles of radiation physics. In R. T. Hoppe, T. L. Phillips, and M. Roach, editors, *Leibel and Phillips Textbook of Radiation Oncology (Third Edition)*, pages 95–119. W.B. Saunders, Philadelphia, third edition edition, 2010.